HETEROGENEOUS PHOTO-FENTON OXIDATION OF BENZOIC ACID IN WATER: EFFECT OF OPERATING CONDITIONS, REACTION BY-PRODUCTS AND COUPLING WITH BIOLOGICAL TREATMENT

M. Isabel Pariente[a,*], *Fernando Martínez*[a], *Juan Antonio Melero*[a], *Juan Ángel Botas*[a], *Theodora Velegraki*[b], *Nikolaos P. Xekoukoulotakis*[b], *Dionissios Mantzavinos*[b]

[a] Department of Chemical and Environmental Technology, ESCET, Rey Juan Carlos University, 28933 Móstoles, Madrid, Spain

[b] Department of Environmental Engineering, Technical University of Crete, Polytechneioupolis, GR-73100 Chania, Greece

Published on: Applied Catalysis B: Environmental 85 (2008) 24-32.

doi:10.1016/j.apcatb.2008.06.019

[*]To whom correspondence should be addressed

Tel: 0034 91 664 74 93; Fax:0034 488 70 68; e-mail: isabel.pariente@urjc.es

Abstract

The heterogeneous photo-Fenton oxidation of benzoic acid, a precursor of several organic pollutants found in agro-industrial effluents, was studied in model aqueous solutions. UVA irradiation was provided by a 125 W medium pressure mercury lamp, while a nanocomposite material of crystalline iron oxides supported over mesostructured SBA-15 was used as the catalyst. Experiments were conducted at benzoic acid initial concentrations between 25 and 450 mg/L, catalyst concentrations between 0.3 and 1.2 g/L and hydrogen peroxide concentrations between 20% and 100% of the stoichiometric amount needed for complete mineralization. Conversion, which was found to be first order regarding benzoic acid concentration, generally increased with increasing the concentration of Fenton's reagents and decreasing substrate concentration. HPLC analysis showed that oxidation was accompanied by the formation of several by-products; of these, the three monohydroxybenzoic acids as well as oxalic acid were successfully identified and quantified. By-products were more resistant to oxidation than benzoic acid since COD reduction was generally lower than substrate conversion. Catalyst stability was assessed measuring the extent of iron leaching in the reaction mixture and was found to be excellent as dissolved iron never exceeded 5% relative to the initial iron content. The aerobic biodegradability of benzoic acid before and after photo-Fenton oxidation was assessed by shake flask tests. Chemical oxidation enhanced the biodegradability of benzoic acid although the oxidized solution was more ecotoxic to marine bacteria than the original one. The feasibility of coupling chemical and biological oxidation was also assessed for an actual olive oil mill effluent.

Keywords: photo-Fenton, heterogeneous catalyst, SBA-15, benzoic acid, OMW, AOP

1. Introduction

Effluents originating from agro-industrial and food-processing activities usually contain several classes of phenolic compounds that exhibit low biodegradability and/or increased toxicity. These compounds are usually classified in three main families, namely (i) cinnamic acid derivatives, (ii) benzoic acid derivatives and (iii) tyrosol related-compounds. Several studies have proven the negative effect of these compounds on land [1] and water [2] environments. Over the past several years, advanced oxidation processes have emerged as efficient technologies for the destruction of various classes of biorecalcitrant aromatic pollutants in waters. Of the various processes, the Fenton's reaction offers a simple and cost-effective source of hydroxyl radicals since its reagents are inexpensive, environmentally benign and relatively easy to transport and handle [3]. Moreover, process efficiency may be enhanced in the presence of UV-Vis irradiation since photolysis of Fe^{3+} promotes Fe^{2+} regeneration [4].

The application of Fenton and photo-Fenton processes based on homogeneous ferrous or ferric salts usually suffers two major drawbacks associated with (i) the narrow pH range of operation, typically between 2.5 and 3.5, to avoid the formation and subsequent precipitation of iron oxyhydroxides and (ii) the need to recover dissolved ions from the treated solution, thus requiring an additional treatment stage. In this respect, the immobilization of Fenton's catalyst on a heterogeneous matrix would enable its use under non-controlled pH conditions as well as its easy recovery from the treated effluent. Several iron-containing materials have been studied for the degradation of model compounds in batch photochemical reactors, such as zeolitic Fe(III)-Y and Fe(II)-3X materials [5], perfluorosulphonic Nafion polymers [6] and pillared clays [7]. The low exchange of iron species within the zeolite framework and its poor stability are the main drawbacks of these microporous materials. The presence of sulphonic acid groups in the polymeric matrix makes Nafion a good candidate for the anchoring of active iron ions in form of films or pellets. The main limitation of this catalytic system has been associated with the relative high cost of the perfluorosulphonic polymer. The

interlamelar structure of pillared clays by the intercalation of large polyoxocations of iron that can be thermally transformed in oxides grafted to the clays layers have revealed a low deactivation due to iron leaching accompanied with remarkable results in terms of the pollutant abatement. Iron-containing mesoporous materials based on supporting Fe_2O_3 particles over hexagonally pore channels of mesostructured SBA-15 silica support have resulted in a very promising catalyst as compared to other photo-Fenton catalysts supported over different types of silica like amorphous xerogels and microporous zeolite materials [8]. It was determined that the physicochemical properties of Fe_2O_3/SBA-15 materials, with an extended surface area and pore distributions within the mesophase range, were responsible for high degradation rates of phenol in photo-assisted Fenton-like processes. In fact, it has been demonstrated that the photo-activity of a catalyst can be strongly influenced by its surface area, crystal structure, particle size distribution or surface hydroxyl group density [9].

The degradation of a model aqueous solution of benzoic acid by heterogeneous photo-Fenton oxidation using solid Fe_2O_3/SBA-15 catalyst has been studied in this work. Benzoic acid constitutes the parent molecule of many phenolic compounds such as vanillic, gallic, veratric, syringic, protocatechuic and hydroxybenzoic acids that are commonly found in agro-industrial effluents. In the form of its ester, benzoic acid is also widely used in the food and pharmaceutical industry as an antimicrobial preservative frequently included in liquid forms and personal care products. To the best of our knowledge, most of studies dealing with photo-Fenton processes were focused on homogeneous catalytic systems. Fewer studies have dealt with heterogeneous iron-supported catalysts for the treatment of single benzoic acid or wastewaters containing derivatives such as those coming from olive mill wastewater (OMW). Thiruvenkatachari et al. [10] demonstrated an efficient 80% benzoic acid conversion within 30 min of reaction by homogeneous photo-Fenton systems; additionally, coupling of photo-Fenton oxidation with ozonation led to its complete degradation within 10 min. Andreozzi and Marotta [11] also investigated the activity of Fe^{3+}/air/UV (i.e. without hydrogen peroxide) for

benzoic acid degradation and developed a comprehensive kinetic model. Regarding heterogeneous catalytic systems, TiO_2 has been employed for the degradation benzoic acid under different operating conditions (i.e. loading of the photocatalyst, solution pH and initial concentration of substrate), demonstrating the potential application of photocatalysis for low organic contents of the synthetic model wastewater [12]. Both TiO_2 photocatalysis and homogeneous photo-Fenton systems have also been tested for the treatment of OMW, with photo-Fenton being more effective reaching 100% and 85%, respectively, of phenols and COD removal for different OMW wastewaters [13].

This work has been focused on the evaluation of different operating conditions, such as catalyst loading, initial hydrogen peroxide and pollutant concentrations, for the photo-Fenton degradation of benzoic acid using a silica-supported iron catalyst in order to improve (i) process efficiency in terms of benzoic acid and COD reduction, and (ii) the effect of chemical oxidation on sample's aerobic biodegradability and toxicity.

2. Materials and methods

2.1. Catalyst and chemicals

Powder iron-containing SBA-15 mesostructured material was synthesized by co-condensation of iron ($FeCl_3 \cdot 6H_2O$, Aldrich) and silica (tetraethoxysilicate, 98%, Aldrich) sources templated with Pluronic 123 (MW=5800, BASF) under acidic conditions as described elsewhere [14]. The resulting catalyst consists of crystalline hematite particles embedded into a mesoestructured silica support with ca. 16% of iron content in the bulk sample. The silica matrix is characterized by typical hexagonal arrangement of mesostructured SBA-15 materials, leading to highly extended surface areas (S_{BET} ca. 500 m^2/g) with a narrow pore diameter within the mesoporous range (6-7 nm). More details about preparation and

characterization of iron-containing SBA-15 mesostructured material were described elsewhere [8].

2.2. Characterization of Catalyst

X-ray powder diffraction data were acquired on a PHILIPS X-PERT diffractometer using Cu Ka radiation. The data were collected from 2θ ranging from 0.5º to 90º with a resolution of 0.02º. Nitrogen adsorption and desorption isotherms at -196ºC were measured using a Micromeritics Tristar 3000 equipment. The data were analysed using the t-plot and BET methods for the estimation of microporous, mesoporous and total surface areas. Bulk iron content of the prepared sample was obtained by atomic emission spectroscopy with induced coupled plasma (ICP–AES) analysis collected in a Varian Vista AX system.

2.3. Photo-Fenton experiments

Photocatalytic experiments were conducted in an immersion well, batch type, laboratory scale photoreactor (350 mL of working volume), purchased from Ace Glass (Vineland, NJ, USA). It is a three compartment apparatus and consists of an inner, double-walled, borosilicate glass housing the lamp and an external cylindrical reaction vessel joined together with an internally threaded connection with the aid of a nylon bushing connector and an O-ring. The optical pathlength of the reactor was 1.1 cm. The reaction mixture was placed in the external cylindrical reaction vessel and the inner double-walled borosilicate glass was immersed inside the reaction mixture. A 125 W, medium pressure mercury vapor lamp (Osram HQL MBF-U), which emits predominantly at 365 nm, was located inside the inner borosilicate glass and was effectively cooled by a water circulation stream through the double-walled compartment, acting as a cooling water jacket. The incident radiation in the solution measured by ACCU-CAL-50 radiometer (DYMAX Corporation) within the UV region was 28 mW cm^{-2}**.** During photocatalytic experiments, temperature was maintained at 27±3ºC. The external reaction

vessel was covered with aluminum foil to reflect irradiation exerting the outer wall of the reaction vessel.

In a typical run, the iron-containing catalyst was dispersed in the liquid and the lamp was switched on. The reactor contents were magnetically stirred, while air was continuously sparged in the liquid acting as co-oxidant. The appropriate amount of hydrogen peroxide was then added and this was taken as zero reaction time. The initial pH of the solution was about 3.1 and it was left uncontrolled during the experiment reaching values of about 4.0-4.5 at the end of the experiment. Samples periodically drawn from the reactor were analyzed with respect to various properties.

All organics used for photo-Fenton reactions, i.e. benzoic acid ($C_7H_6O_2$, ≥ 99.5 %), 4-hydroxybenzoic acid ($C_7H_6O_3$, 99 %), 3-hydroxybenzoic acid ($C_7H_6O_3$, ≥ 98 %), 2-hydroxybenzoic acid ($C_7H_6O_3$, ≥ 99 %), gallic acid monohydrate ($C_7H_6O_5 \cdot H_2O$, ≥ 98%), p-coumaric acid ($C_9H_8O_3$, ≥ 98 %) and oxalic acid ($C_2H_2O_4$, 98 %) were purchased from Fluka. Hydrogen peroxide in the form of 35% w/w solution was provided by Merck. The actual OMW was collected from a three-phase continuous olive oil mill located at Chania, W. Crete, Greece.

2.4. Shake flask tests

Shake flasks experiments were performed to assess the aerobic biodegradability of benzoic acid and OMW samples prior to and following photo-Fenton treatment. Flasks containing 150 mL of the corresponding solution were first neutralized with the appropriate amount of NaOH, then added 2 mL of activated sludge taken from the municipal wastewater treatment plant of Chania, W. Crete, Greece and shaken at 150 rpm and ambient temperature. As hydrogen peroxide can affect the biological action of microorganisms, the residual H_2O_2 concentration was quenched adding MnO_2 which was then separated by filtration. Samples periodically

drawn from the flasks were filtered with a 0.5 μm disposable filter and analyzed with respect to their dissolved COD.

2.5. Analytical techniques

High performance liquid chromatography (HPLC) was used to determine the concentration of reactants (benzoic, 4-hydroxybenzoic, gallic and p-coumaric acids) as well as reaction intermediates such as 2-, 3-, 4-hydroxybenzoic and oxalic acids. Analysis was performed at 30ºC on a Shimazu10A apparatus comprising two LC-10ADVp pumps, an autosampler (SIL-10ADVp) and a SPD-M10AVp diode array detector (DAD). A reverse-phase C-18 column (4.6 mm x 250 mm; Prevail Organic Acid) was used as stationary phase. Acidified water (pH of about 2.5) and acetonitrile were eluted as mobile phases. The flowrate was kept at 1 mL/min and the injection volume was 20 μL. Chemical oxygen demand (COD) tests were performed by digestion of solutions prepared with the addition of 2 mL of sample into commercially available solution containing potassium dichromate, sulphuric acid and mercuric sulphate (Hach Europe, Belgium). The resulting solution was incubated for 120 min at 150ºC in a COD reactor (Model 45600-Hach-Company, USA). Thereafter, COD was determined colorimetrically using a DR/2010 spectrophotometer (Hach Company, USA). Residual hydrogen peroxide concentration was determined using Merckoquant paper strips (Merck). This method was used to evaluate semi-quantitatively the overall H_2O_2 consumption as well as its total conversion prior to any bioassays. The extent of iron dissolution in the liquid phase from the supported catalyst was measured by atomic absorption spectroscopy on an Analytic Jena AAS-6 Vario instrument. The luminescent marine bacteria *V. fischeri* were used to assess the acute ecotoxicity of benzoic acid and OMW samples prior to and following photo-Fenton treatment. The inhibition of *V. fischeri* exposed to treated and untreated samples for 30 min at 15ºC was measured using a LUMIStox analyzer (Dr Lange, Germany) and the results were compared to an aqueous control with color correction. The pH of the samples was

adjusted to 6.5-7.5 prior to toxicity tests, so that pH-related light inhibition was ruled out. Moreover, salt was added to each sample (2% NaCl) to exclude light inhibition due to osmotic phenomena.

3. Results and discussion

3.1. Effect of hydrogen peroxide concentration

Figure 1 shows benzoic acid photo-Fenton conversion-time profiles as a function of initial H_2O_2 concentration at 50 mg/L benzoic acid and 0.6 g/L catalyst concentrations. H_2O_2 concentration was varied between 42 and 210 mg/L with these values corresponding to 20 and 100% of the stoichiometric amount needed for the complete mineralization of benzoic acid, according to eqn (1):

$$C_7H_6O_2 + 15 \cdot H_2O_2 \rightarrow 7 \cdot CO_2 + 18 \cdot H_2O \qquad (1)$$

As seen in Figure 1, the rate of benzoic acid conversion increases with increasing oxidant concentration during the early stages of reaction; nonetheless, 85% conversion and complete degradation was achieved after 120 and 240 min of reaction respectively for 84 mg/L oxidant concentration (this corresponds to 40% of the stoichiometric amount). Similar conversions were also achieved for higher oxidant concentrations, while for the run carried out at 42 mg/L concentration, benzoic acid conversion was 70 and 90% respectively after 120 and 240 min. An additional run was performed without hydrogen peroxide leading to marginal benzoic acid removal.

Table 1 shows final (i.e. after 240 min) values of benzoic acid, COD and hydrogen peroxide conversion for the runs shown in Figure 1. In addition to complete benzoic acid conversion, significant COD reductions between 65 and 90% were recorded for oxidant concentrations in the range 84-210 mg/L, thus indicating that benzoic acid is converted to other more oxygenated reaction by-products which are eventually mineralized to CO_2 and H_2O.

Interestingly, increasing oxidant concentration from 126 to 168 or 210 mg/L had an adverse effect on COD removal which decreased from 90 to about 75-80%.

The last column of Table 1 shows the ratio of the concentration of removed COD over the amount of consumed oxidant, which is an indicator of the efficient oxidant utilization. A low value of this parameter indicates that hydrogen peroxide is not effectively utilized to generate reactive hydroxyl radicals that can further attack the organic compounds. As seen in Table 1, the efficiency of oxidant utilization for COD removal is maximized at 40-60% concentration, while at higher concentrations it drops substantially accompanied by a decrease in COD removal. This could be due to hydrogen peroxide not selectively being converted to hydroxyl radicals and/or, once radicals have been generated, they are wasted through scavenging reaction mechanisms. During photo-Fenton reactions, it has been demonstrated that hydroxyl radicals can partly be scavenged by hydrogen peroxide (particularly at increased oxidant concentrations) to form hydroperoxyl radicals (eqn (2)) with a lower oxidizing power [15]; the latter can also scavenge hydroxyl radicals according to eqn (3):

$$H_2O_2 + HO^{\bullet} \rightarrow HO_2^{\bullet} + H_2O \quad (2)$$

$$HO_2^{\bullet} + HO^{\bullet} \rightarrow H_2O + O_2 \quad (3)$$

Hence, 60% of the stoichiometric amount has been considered a satisfactory initial oxidant concentration to achieve an acceptable catalytic performance with a complete benzoic acid conversion, a substantial COD reduction and an efficient oxidant consumption.

3.2. Effect of catalyst concentration

Figure 2 shows benzoic acid photo-Fenton conversion-time profiles as a function of catalyst concentration in the range 0.3-1.2 g/L at 50 mg/L benzoic acid and 126 mg/L hydrogen peroxide concentrations (this is 60% of the stoichiometric amount). Table 2 also shows final values (i.e. after 240 min) of benzoic acid, COD and oxidant conversions. As seen, the initial

benzoic acid degradation rate increases with increasing catalyst concentration; however, complete conversion was achieved after 240 min of reaction regardless catalyst concentration. On the other hand, catalyst concentration had a more pronounced effect on final COD removal which increased from 73 to 88% increasing catalyst from 0.3 to 0.6 g/L, thus implying that reaction by-products are more recalcitrant to oxidation than the initial substrate. In Figure 2 and Table 2 are also included the results of an additional experiment performed without catalyst in the presence of hydrogen peroxide. In this case, about 66% benzoic acid conversion and 16% COD removal were achieved after 240 min of reaction. The same run was carried out in the absence of hydrogen peroxide showing negligible degradation of benzoic acid by UV radiation itself. These results seem to indicate the partial degradation of benzoic acid as a result of the production of reactive radicals by the photolysis of hydrogen peroxide (eqn (4)). It should be noted that marginal irradiation emitted by the UV lamp at wavelengths between 320 and 290 nm enables the photolysis of hydrogen peroxide. This is in agreement with the 20% hydrogen peroxide conversion detected at 240 min for this experiment. From these results, the active role of Fe_2O_3/SBA-15 in combination of hydrogen peroxide for the degradation of benzoic acid is demonstrated.

$$H_2O_2 + hv \rightarrow 2HO^{\bullet} \quad (4)$$

On the other hand, previous results reported by Martínez et al. [16] revealed a significant contribution of dark-Fenton reactions to the overall catalytic degradation of photo-Fenton systems, in particular under high hydrogen peroxide and catalyst loadings. In order to determine this possible contribution, two additional experiments using 50 mg/L benzoic acid and 0.6 g/L catalyst concentrations under dark reaction conditions were carried out: (i) without hydrogen peroxide (dark adsorption) and (ii) in the presence of 126 mg/L hydrogen peroxide (dark Fenton). Dark adsorption onto the catalyst surface was responsible for about 10% benzoic acid removal**.** The contribution of dark Fenton reactions was moderate leading to about 64% and 14% benzoic acid and COD removal, respectively, after 240 min; the

281 respective values for the photo-Fenton run were 100% and 88%, thus confirming the strong
282 influence of UV radiation on Fenton's reactivity for benzoic acid degradation.
283 To assess the stability of catalyst under reaction conditions, samples were analyzed regarding
284 the concentration of dissolved iron ions and the results are summarized in Table 2. Leached
285 iron concentration was between 1.1 and 3.6 mg/L depending on the catalyst loading; these
286 values correspond to less than 5% of the iron content of the fresh catalyst. A plausible
287 explanation of the iron leaching for hematite iron oxide in photocatalytic systems has been
288 already suggested elsewhere [17]. It was reported that Fe_2O_3 in the form of hematite could be
289 reduced to Fe^{2+} over the iron surface lattice due to the adequate potential gradient to separate
290 h^+_{cb} and e^-_{vb} in the presence of UV light (eqns (5) and (6)). In this work it was also proposed
291 the partial dissolution of reduced Fe^{2+} surface lattice to Fe^{3+} ions in the reaction medium via
292 reactions of the positives holes (eqn (7)).

293 $$Fe_2O_3 \rightarrow Fe_2O_3\ (e^-_{cb}, h^+_{vb}) \quad (5)$$

294 $$e^-_{cb} + Fe^{3+}_{surface} \rightarrow Fe^{2+}_{surface} \quad (6)$$

295 $$Fe^{2+}_{surface} + h^+_{vb} \rightarrow Fe^{3+}_{dissolution} \quad (7)$$

296 A sample containing 126 mg/L H_2O_2 and 0.6 g/L catalyst but no benzoic acid was irradiated
297 for 240 min to check for the stability of Fe_2O_3/SBA-15; interestingly, the leached iron
298 concentration was lower than 0.1 mg/L. This result clearly evidences that leaching of
299 Fe_2O_3/SBA-15 is associated with the potential capacity of benzoic acid and/or by-products
300 when they are oxidized over the catalyst surface producing stable soluble metallic organic
301 complexes that are dissolved in the reaction medium (i.e iron oxalate complex). This
302 hypothesis has been already proposed to account for the metal leaching of supported catalysts
303 in catalytic wet peroxide [18] and wet air oxidation [19] studies. In this sense, the degradation
304 of benzoic acid is predominantly attributed to the hydroxyl radicals (HO•) generated by
305 Fenton reactions over the catalyst surface (eqns (8-10)). These hydroxyl radicals would be

responsible for the oxidation of adsorbed organic compounds in the surroundings of catalyst surface.

$$Fe^{3+}(OH^-) + hv \rightarrow Fe^{2+} + HO^{\bullet} \quad (8)$$

$$Fe^{3+} + H_2O_2 \rightarrow Fe^{2+} + H^+ + HO_2^{\bullet} \quad (9)$$

$$Fe^{2+} + H_2O_2 \rightarrow Fe^{3+} + OH^- + HO^{\bullet} \quad (10)$$

Taking into account the proposed oxidation scheme, the efficiency of the active iron sites supported over silica supports is associated with the oxidant decomposition and the catalyst capacity for the adsorption-desorption of both oxidant and organic compounds. The immobilization of iron oxides over mesostructured materials with an extended surface area is of outstanding importance in order to enhance their catalytic properties.

To evaluate the contribution of dissolved iron to the degradation, a sample containing 50 mg/L benzoic acid, 126 mg/L hydrogen peroxide and 0.6 g/L catalyst was irradiated for 240 min. The resulting solution was filtered to remove the solid catalyst and then added fresh benzoic acid and hydrogen peroxide to 50 and 126 mg/L concentration respectively. This solution which already contained about 3 mg/L dissolved iron from the previous run was again irradiated in the absence of Fe_2O_3/SBA-15. Interestingly, complete benzoic acid degradation was recorded after 180 min of reaction which is comparable to the performance of the respective catalytic run (see Figure 2). However, the extent of COD removal after 240 min was only 32%, while the value of the respective catalytic run was 88% (see Table 2). From the aforementioned results, it can be deduced that the degradation of benzoic acid and its metabolites cannot be fully ascribed to the heterogeneous activity of Fe_2O_3/SBA-15 catalyst but it is partly due to (i) hydrogen peroxide-induced photolytic reactions and (ii) homogeneous activity associated with dissolved metals.

The physicochemical properties of Fe_2O_3/SBA-15 were also evaluated for a catalyst sample recovered after a photocatalytic run carried out at 50 mg/L benzoic acid, 126 mg/L hydrogen

peroxide and 0.6 g/L catalyst loading. Figure 3 illustrates XRD patterns and nitrogen isotherms at -196ºC for fresh and used catalyst samples. Table 3 summarizes micropore, mesopore and total surface areas estimated from nitrogen isotherms and their iron content for both materials. It is clearly observed the hexagonal arrangement of mesostructured SBA-15 silica as well as diffraction peaks characteristic of hematite crystalline entities for the spent catalyst. In terms of textural properties, insignificant changes can be remarked as a result of the photo-Fenton reaction. The slight decrease of the iron content for the spent catalyst is in agreement with the low iron concentration detected in the aqueous solution. These results reveal a remarkable stability of the Fe_2O_3/SBA-15 catalyst, thus making it a promising catalytic material for this type of environmental applications.

3.3. Effect of initial benzoic acid concentration

The effect of changing benzoic acid concentration in the range 25-450 mg/L on its conversion during photo-Fenton oxidation was studied at 0.6 g/L catalyst concentration and a hydrogen peroxide concentration equal to 60% of the stoichiometric amount needed for complete mineralization. As seen in Figure 4, conversion decreases with increasing initial concentration although, in all cases, complete degradation was achieved after 240 min of reaction. On the other hand, the final (i.e. after 240 min) COD reduction was 92, 88, 72 and 16% for the runs performed at initial benzoic acid concentrations of 25, 50, 150 and 450 mg/L respectively.

Kinetic studies of photo-Fenton processes can be performed assuming that the reaction between hydroxyl radicals and the pollutant is the rate determining step as has been reported by other authors [20]. Thus, benzoic acid degradation may be described by a pseudo-first order kinetic expression:

$$-\frac{dC}{dt} = k \cdot C_{OH^{\bullet}} \cdot C = k_{app} \cdot C \Rightarrow Ln\frac{C_0}{C} = k_{app} \cdot t \quad (11)$$

where C is the benzoic acid concentration, k is the reaction rate constant and k_{app} is a pseudo-first order constant. Figure 5 shows the results of Figure 4 plotted in the form of eqn (11); straight lines passing through the origin fit the experimental data well (the coefficient of linear regression, r, is always greater than 0.98) and from the slopes, k_{app} values of 0.02, 0.017, 0.014 and 0.011 1/min are computed for the runs at 25, 50, 150 and 450 mg/L initial benzoic acid concentration, respectively. It should be noted that linear fitting was done for those reaction times necessary to achieve up to 75% conversion of benzoic acid. This criterion was set assuming a steady state production of hydroxyl radicals from hydrogen peroxide decomposition which is likely to occur mainly during the early stages of the reaction. The fact that the degradation rate decreases with increasing initial concentration may be explained by (i) an increase of the molar extinction coefficients due to the formation of several reaction by-products at considerable concentrations, thus absorbing a substantial portion of the emitted radiation and (ii) less active sites are available at higher substrate concentrations, thus triggering a competitive adsorption onto the catalyst surface [18].

3.4. Determination of reaction by-products

Four intermediate compounds accompanying the photo-Fenton oxidation of benzoic acid, namely 2-, 3- and 4-hydroxybenzoic acids (HBAs) and oxalic acid were positively identified by means of HPLC/DAD analysis. Figure 6 shows concentration-time profiles of all four identified intermediates as well as of the original substrate for the run performed at 50 mg/L benzoic acid, 0.6 g/L catalyst and 126 mg/L hydrogen peroxide concentrations. Hydroxylation of benzoic acid at the ortho-, para- and meta-position may be responsible for the formation of the three HBAs as has also been suggested for the TiO_2-induced photocatalytic degradation of benzoic acid [12]. The formation of dihydroxybenzenes like catechol and hydroquinone is also plausible through decarboxylation of the parent compound or/and HBAs. This pathway has already been proposed for similar structures like phenoxyacetic acid, phenylacetic acid [21]

and 4-hydroxybenzoic acid [22]. However, such intermediates were not detected in this study. Breakdown of the aromatic ring results in the formation of a wide range of cleavage compounds such as low molecular weight carboxylic acids through successive oxidation-decarboxylation cycles.

Oxalic acid was the dominant, in terms of concentration, by-product detected during benzoic acid degradation. Its concentration reached a maximum within the first 15-30 min of reaction (this coincides with about 20-30% benzoic acid conversion) and then decreased presumably due to its fast decarboxylation to carbon dioxide and water. Monohydroxybenzoic acids were detected at trace levels (i.e. <2.5 mg/L), with their maximum concentration appearing between 60 and 120 min (this coincides with about 60-90% benzoic acid conversion). These results indicate that benzoic acid and perhaps other aromatic intermediates undergo fast cleavage to non-aromatic compounds. After 240 min of reaction, all four intermediates as well as benzoic acid do not appear in the reaction mixture; therefore, the remaining organic matter (about 12% COD - see Table 1) can be attributed to unidentified by-products.

3.5. Degradation of benzoic acid derivatives

In further studies, the photo-Fenton oxidation of two benzoic acid derivatives, namely 4-hydroxybenzoic and gallic (3,4,5-trihydroxybenzoic) acids was studied at 50 mg/L initial substrate concentration, 0.6 g/L catalyst concentration and an hydrogen peroxide concentration of 60% of the stoichiometric amount. Figure 7 shows the respective conversion-time profiles, while Table 4 summarizes the respective substrate, COD and hydrogen peroxide conversions as well the apparent pseudo-first order rate constants computed for each compound according to equation 12 (for up to 75% conversion). As seen, reactivity decreases in the order gallic acid>4-hydroxybenzoic acid>benzoic acid, i.e. decreases with decreasing number of electron-donating groups. The presence of such groups facilitates the electrophilic attack of the aromatic ring by hydroxyl radicals [23, 24] and this is more pronounced for gallic acid

(bearing three electron-donating groups) which was rapidly oxidized within the first 15 min of reaction (thus not allowing the accurate calculation of its rate constant).

An additional run was performed with 4-coumaric (4-hydroxycinnamic) acid which belongs to the cinnamic acid derivatives typically found in agro-industrial effluents and the results are also included in Figure 7 and Table 4. 4-Coumaric acid is evidently more susceptible to oxidation than 4-hydroxybenzoic acid (its counterpart from the benzoic acid family), indicating that the exocyclic double bond in cinnamic acid derivatives increases their reactivity during the photo-Fenton process. This was also the case with cinnamic acid whose oxidation rate was twice as fast as that of benzoic acid (data not shown).

3.6. Aerobic biodegradability

To assess the effect of photo-Fenton oxidation on aerobic biodegradability, solutions containing 150 and 450 mg/L of benzoic acid were subject to oxidation for 240 min at 0.6 g/L catalyst concentration and a hydrogen peroxide concentration of 60% of the stoichiometric amount and the resulting reaction mixtures were inoculated with activated sludge in shake flask tests. In parallel, the untreated solutions were also inoculated with activated sludge under identical conditions. Figure 8 shows COD conversion-time profiles throughout the duration of biological tests.

Photo-Fenton oxidation resulted in 72% and 16% COD reduction at 150 and 450 mg/L benzoic acid concentration, respectively. When the original, unoxidized samples were subject to direct aerobic biodegradation, the respective values after 12 days of incubation were 30% and 37%, thus implying low biodegradation rates. Nevertheless, coupling photo-Fenton oxidation with aerobic post-oxidation led to 77% and 69% overall COD removal at 150 and 450 mg/L, respectively. The beneficial effect of process combination was more pronounced for the test with the highest benzoic acid concentration although a relatively low COD

reduction was accomplished for the photo-Fenton step. On the other hand, this synergy was less evident at 150 mg/L benzoic acid concentration since, at the conditions in question, most of the organic content was already removed in the previous chemical oxidation step. Interestingly, although oxidized by-products seem to be more readily degradable aerobically than benzoic acid itself, they are also more ecotoxic to *V. fischeri* bacteria. The luminescent inhibition of benzoic acid to marine bacteria was 9% and 25% at 150 and 450 mg/L concentration, respectively, in contrast to samples after photo-Fenton oxidation where values increased to 87% and 83%, respectively. Similar results have recently been reported by Oller et al. [25] who found that solar photo-Fenton treatment of pesticides-containing solutions enhanced their aerobic degradability although it increased their ecotoxicity to *V. fischeri*. The authors suggested that this was due to the fact that activated sludge treatment is far more robust than ecotoxicity tests to the presence of recalcitrant compomds. In our work, increased toxicity cannot be ascribed to unreacted oxidant because it was removed prior to toxicity and biodegradability tests. However, the possibility that increased toxicity is partly due to dissolved iron cannot be discarded.

In a final set of experiments, the feasibility of coupling chemical and biological oxidation was assessed for a real agro-industrial effluent from olive oil processing (OMW). The effluent was first subject to filtration to separate its solids and then diluted with water to achieve an initial concentration of 1400 mg/L COD. OMW was then subject to photo-Fenton oxidation at 0.6 g/L catalyst concentration and 1900 mg/L hydrogen peroxide concentration; this corresponds to 60% of the oxidant stoichiometric amount needed for the complete mineralization of OMW organic matter assuming that COD is only due to benzoic acid. Following oxidation for 240 min, which led to 34% COD removal, the effluent was inoculated with activated sludge; similarly, the untreated OMW was also inoculated with activated sludge under identical conditions. COD-conversion time profiles for both the untreated and oxidized effluents are shown in Figure 8. Direct biological oxidation resulted in 68% COD removal after 12 days of

incubation, while the respective overall value for the combined treatment was 75%. Although both the original and oxidized samples were strongly ecotoxic (89% and 78% inhibition respectively), they were relatively readily biodegradable aerobically with their COD degradation profiles being nearly identical. As ecotoxicity of oxidized OMW cannot be attributed to residual oxidant and/or the iron leached from the catalyst because unconverted hydrogen peroxide was removed prior to toxicity/biodegradability tests and the dissolved iron concentration detected in this case was very low (0.2 mg/L), it is most likely associated with the complex organic matrix and increased COD content of OMW.

HPLC chromatograms of the original OMW and samples taken after photo-Fenton and combined photo-Fenton and biological oxidation are shown in Figure 9. As clearly seen, most of the chromatographic peaks initially present in the effluent successively disappear through photo-Fenton pre-oxidation and aerobic post-treatment. In this view, a combined photochemical-biological system may be a promising alternative for agro-industrial wastewaters treatment.

4. Conclusions

The conclusions drawn from this study can be summarized as follows:

(1) The UVA-induced Fenton oxidation over a supported iron oxide (Fe_2O_3/SBA-15) is capable of degrading readily benzoic acid, a precursor of organic pollutants found in agro-industrial effluents, in model aqueous solutions.

(2) Degradation efficiency, both in terms of substrate conversion and COD reduction, is influenced by several factors such as hydrogen peroxide concentration, catalyst loading and initial substrate concentration. The immobilization of hematite iron oxide over mesostructured silica support with an extended surface area seems to be of outstanding relevance for its catalytic performance.

(3) Benzoic acid degradation, which follows first order kinetics, occurs through the formation of aromatic and ring-cleavage intermediates that, in general, are more stable and ecotoxic than the starting molecule as evidenced by the residual COD of treated solutions and increased acute ecotoxicity values.

(4) Benzoic acid derivatives and alike compounds are also susceptible to photo-Fenton oxidation; their reactivity depends on the number and type of functional groups attached to the aromatic ring.

(5) Photo-Fenton oxidation improves the aerobic biodegradability of benzoic acid as assessed by shake flask tests and this is also the case with an actual agro-industrial effluent. The implication is that photocatalysis may be part of a process train for the effective treatment of this type of industrial effluents.

Acknowledgements

The authors thank "Ministerio de Ciencia y Tecnología" for the financial support through the project CONSOLIDER-INGENIO 2010 and "Comunidad de Madrid" through the project P-AMB-000395-0505. Thanks are due to E. Diamadopoulos for his assistance with AA analysis.

References

[1] M.J. Paredes, E. Moreno, A. Ramos-Cormenzana, J. Martínez, Chemosphere 16(7) (1987) 1557–1564.

[2] M. Della Greca, P. Monaco, G. Pinto, A. Pollio, L. Previtera, F. Temussi, Environ. Contam. Tox. 67(3) (2001) 352–359.

[3] A. Yaping, H. Jiangyong, Appl. Catal. B: Environ. 78(3-4) (2008) 250-258.

[4] J.J. Pignatello, Environ. Sci. and Technol. 26(5) (1992) 944-951.

[5] M. Rios-Enriquez, N. Shahin, C. Durán-de-Bazúa, J. Lang, E. Oliveros, S.H. Bossmann, A.M. Braun, Sol. Energy 77(5) (2004) 491-501.

[6] J. Fernández, J. Bandara, A. López, Ph. Buffat, J. Kiwi, Langmuir 15(1) (1999) 185-192.

[7] S. Azabou, W. Najjar, A. Gargoubi, A. Ghorbel, S. Sayadi,. Appl. Catal. B: Environ. 77(1-2) (2007) 166-174.

[8] F. Martínez, G. Calleja, J.A. Melero, R. Molina, Appl. Catal. B: Environ. 70(1-4) (2007) 452-460.

[9] D.W. Bahnemann, Photochemical Conversion and Storage of Solar Energy, E. Pelizzetti, M. Schiavello (Eds.), Kluwer Academic Publishers, Dordrecht, 1991.

[10] R. Thiruvenkatachari, T.O. Kwon, I.S. Moon, J. Environ. Sci. Health Part A. 41(8) (2006) 1685-1697.

[11] R. Andreozzi, R. Marotta, Water Res. 38(5) (2004) 1225-1236.

[12] T. Velegraki, D. Mantzavinos, Chem. Eng. J. 140(1-3) (2007) 15-21.

[13] W. Gernjak, M.I. Maldonado, S. Malato, J. Cáceres, T. Krutzler, A.Glaser, R. Bauer, Sol. Energy 77(5) (2004) 567-572.

[14] G. Calleja, J.A. Melero, F. Martínez, R. Molina, Water Res. 39(9) (2005) 1741-1750.

[15] F.J. Beltrán, G. Ovejero, J. Rivas, Ind. Eng. Chem. Res. 35(3) (1996) 883-890.

525 [16] F. Martínez, G. Calleja, J.A. Melero, R. Molina, Appl. Catal. B: Environ. 60(3-4) (2005)
526 181-190.
527 [17] C. Pulgarín, J. Kiwi, Langmuir 11(2) (1995) 519-526.
528 [18] J.A. Melero, G. Calleja, F. Martínez, R. Molina, M.I. Pariente, Chem. Eng. J. 131(1-3)
529 (2007) 245-256.
530 [19] Santos A., Yustos P., Quintanilla A., Ruiz G., Garcia-Ochoa F. Appl. Catal. B: Environ.
531 61(3-4) (2005). 323-333.
532 [20] I. Oller, S. Malato, J.A. Sánchez-Pérez, W. Gernjak, M.I. Maldonado, L.A. Pérez-
533 Estrada, C. Pulgarín, Catal. Today 122(1-2) (2007) 150-159.
534 [21] M. Barbeni, C. Minero, E. Pelizeti, E. Borgarello, N. Serpone, Chemosphere 16(10-12)
535 (1987) 2225-2237.
536 [22] F.J. Rivas, F.J. Beltrán, O. Gimeno, J. Frades, J. Agric. Food Chem. 49(4) (2001) 1873-
537 1880.
538 [23] S. Parra, J. Olivero, L. Pacheco, C. Pulgarín, Appl. Catal. B: Environ. 43(3) (2003) 293-
539 301.
540 [24] M.A. Miranda, F. Galindo, A.M. Amat, A. Arques, Appl. Catal. B: Environ. 30(3-4)
541 (2001) 437-444.
542 [25] I. Oller, S. Malato, J.A. Sánchez-Pérez, M.I. Maldonado, R. Gassó, Catal. Today 129(1-
543 2) (2007) 69-78.
544

Table 1. Effect of hydrogen peroxide concentration on conversion after 240 min of reaction. Conditions as in Figure 1. Numbers in brackets show oxidant concentration as percentage of stoichiometric amount.

$[H_2O_2]_0$ (mg/L)	$X_{benzoic\ acid}$ (%)	X_{COD} (%)	X_{H2O2} (%)	Efficiency $COD^{abatement} / H_2O_2^{consumed}$
0 (0)	7.6	7.0	-	-
42 (20)	90.9	12.3	88	0.29
84 (40)	100	65.8	99	0.70
126 (60)	100	89.3	96	0.66
168 (80)	100	81.2	85	0.51
210 (100)	100	75.8	86	0.37

Table 2. Effect of catalyst concentration on conversion after 240 min reaction. Conditions as in Figure 2.

[CAT] (g/L)	$X_{benzoic\ acid}$ (%)	X_{COD} (%)	X_{H2O2} (%)	Fe leached (mg/L)	Fe leached (%)	Efficiency $COD^{abatement} / H_2O_2^{consumed}$
0[a]	≈ 0	≈ 0	-	-	-	-
0	66.1	15.7	21	-	-	0.52
0.3	96.8	72.6	92	1.1	3.7	0.56
0.6	100	87.9	93	2.7	4.5	0.66
1.2	100	85.9	92	3.6	3.0	0.65

[a] Experiment carried out in absence of hydrogen peroxide

560

561

562 **Table 3.** Characterization of fresh and used catalyst.

Catalyst	Iron content (w/w %)	S_{BET} (m^2/g)	$S_{micropores}$ (m^2/g)	$S_{mesopores}$ (m^2/g)
Fe_2O_3/SBA-15 (fresh)	19.3	559.7	214.3	195.9
Fe_2O_3/SBA-15 (used)	18.4	568.8	220.7	214.9

563

564

565

566 **Table 4.** Reactivity of benzoic acid and its derivatives. Reaction conditions: [cat] = 0.6 g/L;

567 $[H_2O_2]$ = 60% of the stoichiometric amount; $[Acid]_0$ = 50 mg/L. nd: not determined.

Compound	k_{app} (1/min)	X_{acid} (%)[a]	X_{acid} (%)[b]	X_{COD} (%)**	X_{H2O2} (%)**
Benzoic Acid	0.02	18	100	87.9	93
4-Hydroxybenzoic Acid	0.024	36	100	87.6	100
Gallic Acid	nd	100	100	83.9	100
4-Coumaric Acid	0.038	52	100	98.9	100

[a] Values at 15 min, [b] Values at 240 min

568

569

570 **LIST OF FIGURES**

571

572 **Figure 1.** Effect of hydrogen peroxide concentration on benzoic acid conversion. Reaction
573 conditions: $[Benzoic\ Acid]_0$ = 50 mg/L; [cat] = 0.6 g/L.

574 **Figure 2.** Effect of catalyst concentration on benzoic acid conversion. Reaction conditions:
575 $[Benzoic\ Acid]_0$ = 50 mg/L; $[H_2O_2]_0$ = 60% of the stoichiometric amount.

576 **Figure 3.** Characterization of fresh and used catalyst. (a) XRD analysis, (b) N_2
577 adsorption/desorption isotherms at -196°C.

578 **Figure 4.** Effect of benzoic acid initial concentration on its conversion. Reaction conditions:
579 [cat] = 0.6 g/L; $[H_2O_2]_0$ = 60% of the stoichiometric amount.

580 **Figure 5.** First order kinetics of the degradation of benzoic acid – plot of eqn (3). Other
581 conditions as in Figure 4.

582 **Figure 6.** Concentration-time profiles of benzoic acid and intermediates. Reaction conditions:
583 [cat] = 0.6 g/L; $[H_2O_2]_0$ = 60% of the stoichiometric amount; $[Benzoic\ Acid]_0$ = 50 mg/L.

584 **Figure 7.** Conversion-time profiles of benzoic acid and its derivatives. Reaction conditions:
585 [cat] = 0.6 g/L; $[H_2O_2]_0$ = 60% of the stoichiometric amount; $[Acid]_0$ = 50 mg/L.

586 **Figure 8.** COD conversion-time profiles during aerobic biodegradation of untreated and
587 oxidized benzoic acid solutions and OMW. -■- untreated at 150 mg/L; -●- untreated at 450
588 mg/L; -▲- untreated OMW; -□- oxidized at 150 mg/L; -○- oxidized at 450 mg/L; -Δ- oxidized
589 OMW.

590 **Figure 9.** HPLC chromatograms of raw and treated OMW samples.

591

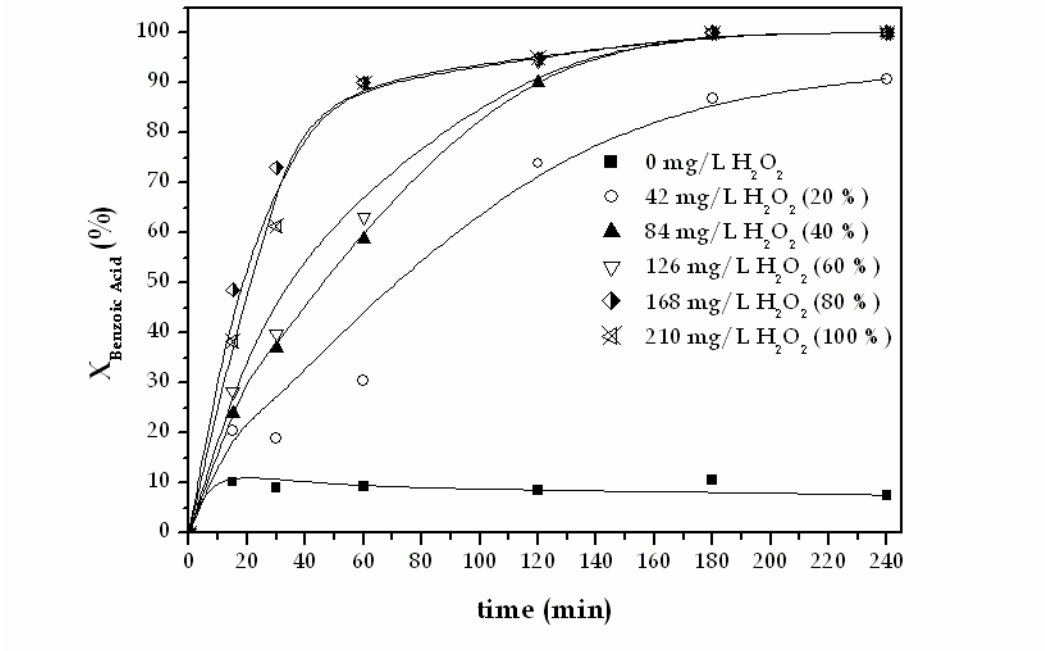

Figure 1

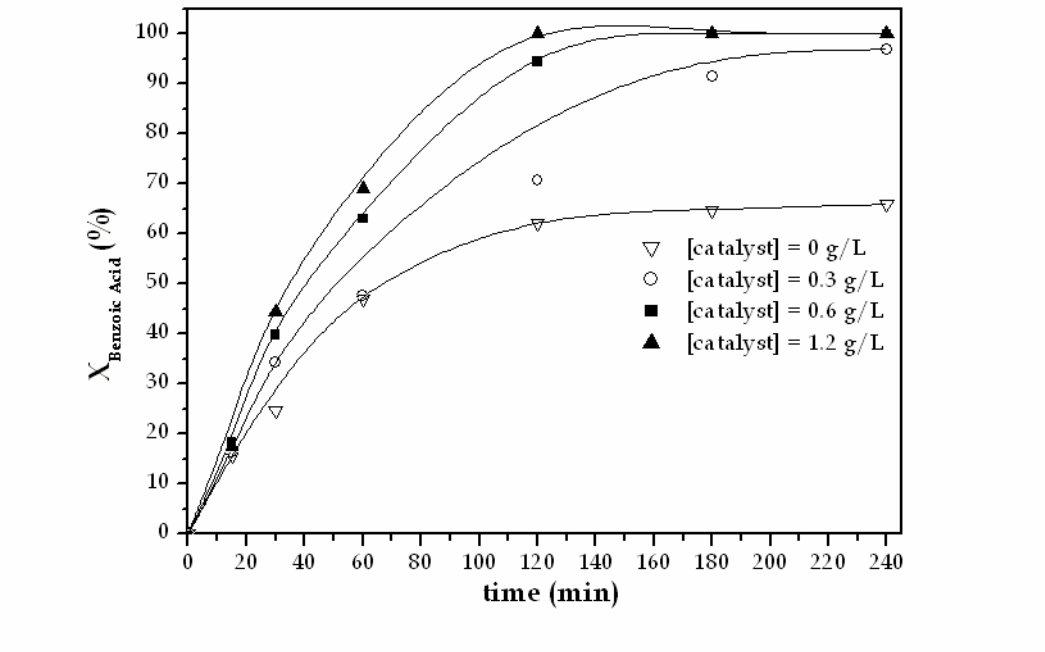

Figure 2

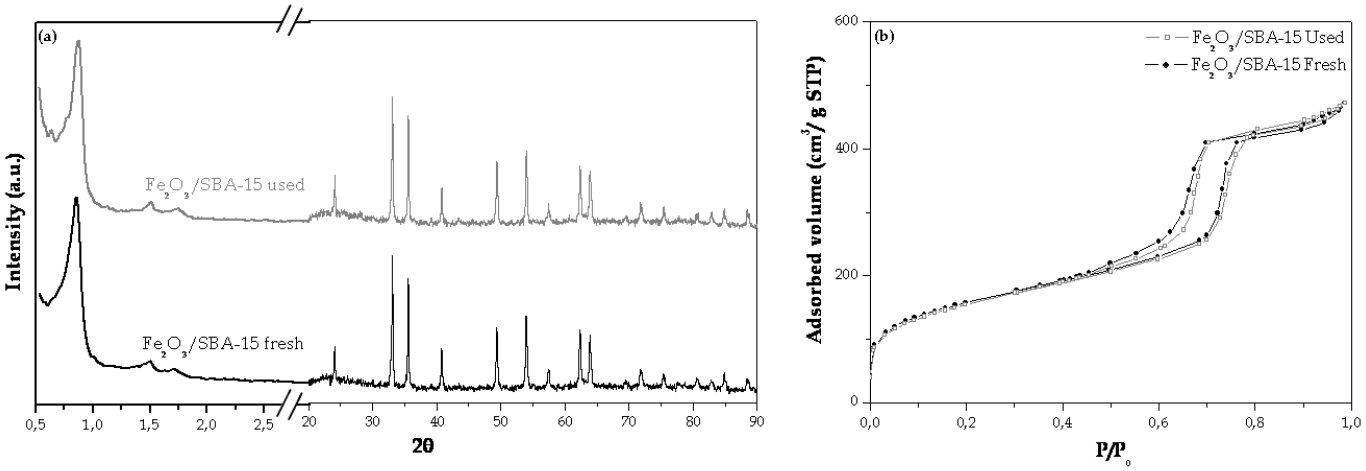

Figure 3

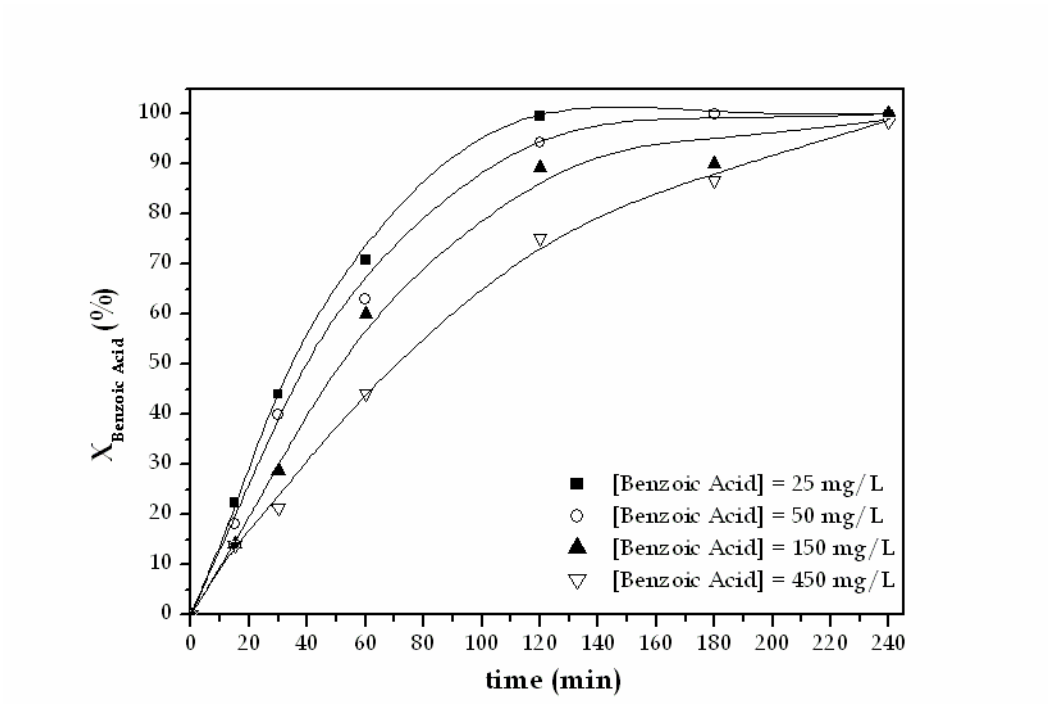

Figure 4

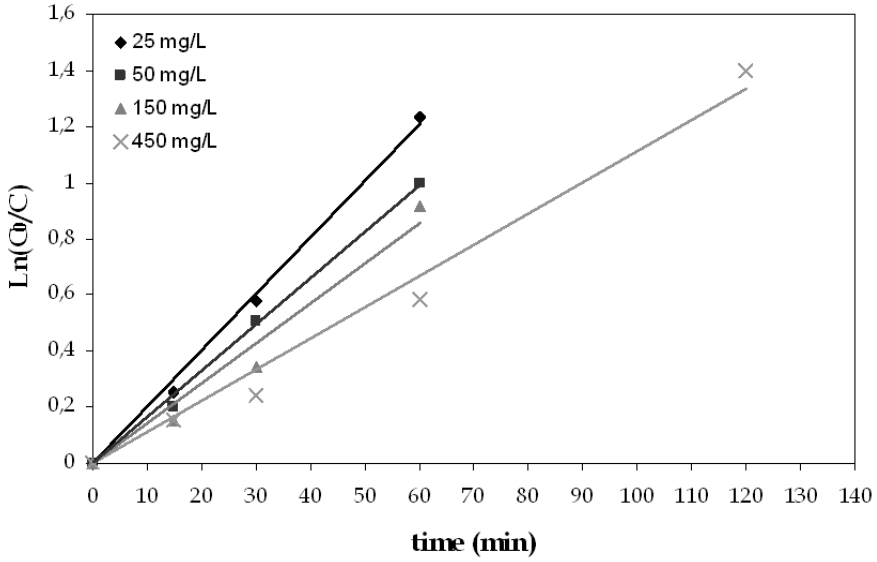

Figure 5

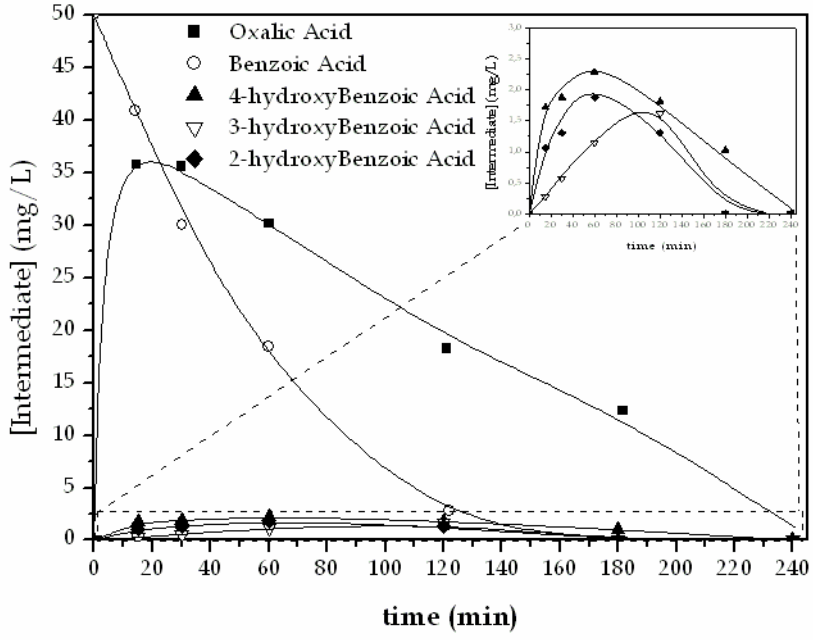

Figure 6

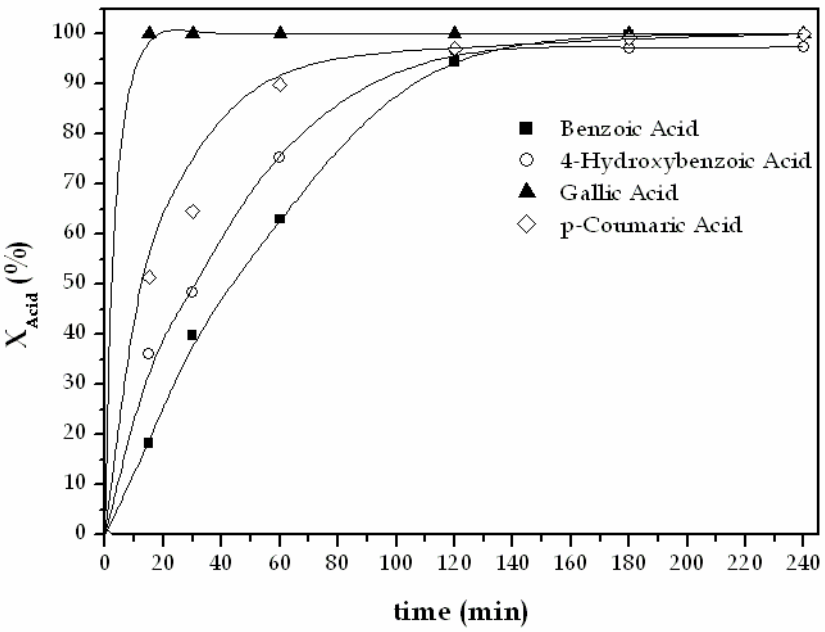

Figure 7

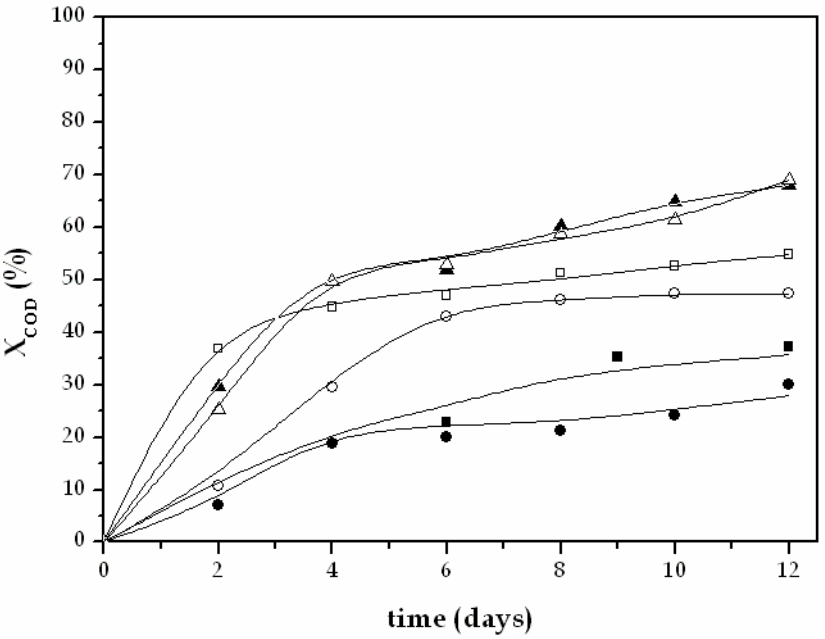

Figure 8

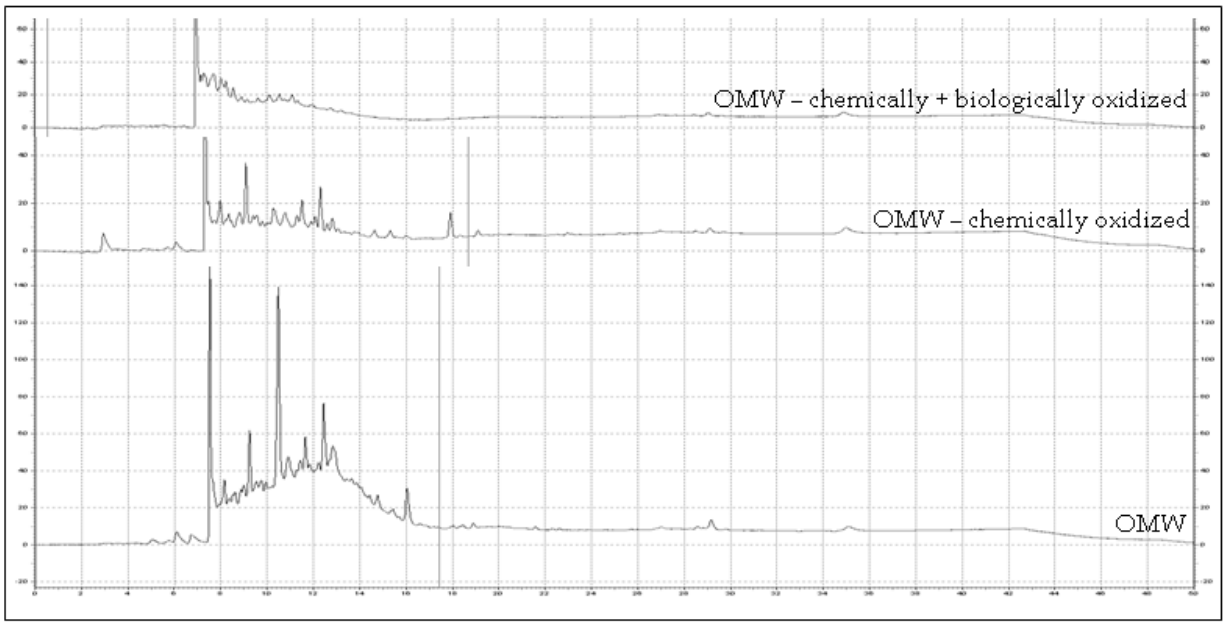
OMW – chemically + biologically oxidized
OMW – chemically oxidized
OMW

Figure 9